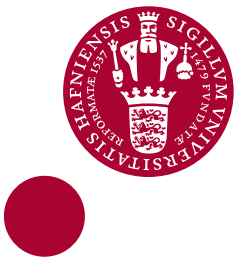

Warburg Effect Metabolism Drives Neoplasia in a Drosophila Genetic Model of Epithelial Cancer

Eichenlaub, Teresa; Villadsen, René; Freitas, Flávia C.P.; Andrejeva, Diana; Aldana, Blanca I.; Nguyen, Hung Than; Petersen, Ole William; Gorodkin, Jan; Herranz, Héctor; Cohen, Stephen M.

Published in:
Current Biology

DOI:
10.1016/j.cub.2018.08.035

Publication date:
2018

Document version
Publisher's PDF, also known as Version of record

Article

Current Biology

Warburg Effect Metabolism Drives Neoplasia in a *Drosophila* Genetic Model of Epithelial Cancer

Highlights

- LDH upregulation is required for the transition from hyperplasia to neoplasia
- LDH expression drives tumor formation in the context of EGFR overexpression
- Increased sugar uptake drives tumor formation in the *Drosophila* EGFR model
- Synergy between EGFR and LDHA correlates with poor outcome in human cancer

Authors

Teresa Eichenlaub, René Villadsen, Flávia C.P. Freitas, ..., Jan Gorodkin, Héctor Herranz, Stephen M. Cohen

Correspondence

hherranz@sund.ku.dk (H.H.), scohen@sund.ku.dk (S.M.C.)

In Brief

Eichenlaub et al. examine gene expression changes during the transition from hyperplasia to neoplasia and identify lactate dehydrogenase as a key driver of neoplasia in a *Drosophila* EGFR model. Elevated sugar flux or a high-sugar diet also drive neoplasia. Synergy between EGFR and LDHA correlates with poor clinical outcome in some human cancers.

Eichenlaub et al., 2018, Current Biology *28*, 3220–3228
October 22, 2018
https://doi.org/10.1016/j.cub.2018.08.035

CellPress

CellPress

Current Biology
Article

Warburg Effect Metabolism Drives Neoplasia in a *Drosophila* Genetic Model of Epithelial Cancer

Teresa Eichenlaub,[1] René Villadsen,[1] Flávia C.P. Freitas,[2,4] Diana Andrejeva,[1] Blanca I. Aldana,[3] Hung Than Nguyen,[1,5] Ole William Petersen,[1] Jan Gorodkin,[2] Héctor Herranz,[1,*] and Stephen M. Cohen[1,6,*]

[1]Department of Cellular and Molecular Medicine, University of Copenhagen, Blegdamsvej 3, Copenhagen 2200 N, Denmark
[2]Center for Non-coding RNA in Technology and Health, Department of Veterinary and Animal Sciences, University of Copenhagen, Grønnegårdsvej 61, 1870 Frederiksberg C, Denmark
[3]Department of Drug Design and Pharmacology, University of Copenhagen, Universitetsparken 2, 2100 Copenhagen, Denmark
[4]Present address: Faculdade de Medicina de Ribeirão Preto, Universidade de São Paulo, Avenida dos Bandeirantes 3900, Ribeirão Preto/SP 14040-901, Brazil
[5]Present address: Department of Pathology, National Cancer Institute, 10 Center Drive, Bethesda, MD 20814, USA
[6]Lead Contact
*Correspondence: hherranz@sund.ku.dk (H.H.), scohen@sund.ku.dk (S.M.C.)
https://doi.org/10.1016/j.cub.2018.08.035

SUMMARY

Cancers develop in a complex mutational landscape. Genetic models of tumor formation have been used to explore how combinations of mutations cooperate to promote tumor formation *in vivo*. Here, we identify lactate dehydrogenase (LDH), a key enzyme in Warburg effect metabolism, as a cooperating factor that is both necessary and sufficient for epidermal growth factor receptor (EGFR)-driven epithelial neoplasia and metastasis in a *Drosophila* model. LDH is upregulated during the transition from hyperplasia to neoplasia, and neoplasia is prevented by LDH depletion. Elevated LDH is sufficient to drive this transition. Notably, genetic alterations that increase glucose flux, or a high-sugar diet, are also sufficient to promote EGFR-driven neoplasia, and this depends on LDH activity. We provide evidence that increased LDHA expression promotes a transformed phenotype in a human primary breast cell culture model. Furthermore, analysis of publically available cancer data showed evidence of synergy between elevated EGFR and LDHA activity linked to poor clinical outcome in a number of human cancers. Altered metabolism has generally been assumed to be an enabling feature that accelerates cancer cell proliferation. Our findings provide evidence that sugar metabolism may have a more profound role in driving neoplasia than previously appreciated.

INTRODUCTION

Cancers develop in a complex mutational landscape [1]. Individual tumors carry hundreds, even thousands, of mutations. Specific tumor types have identifiable signatures, consisting of a small number of relatively common "driver" mutations [2]. The mutational spectrum can vary in different regions of any given tumor, indicating clonal heterogeneity [3, 4]. This heterogeneity poses a challenge to identify which among the many mutational changes contribute to disease.

Genetic models of tumor formation have been used to explore how combinations of mutations can cooperate to promote neoplasia [5–9]. Excess epidermal growth factor (EGF) receptor activity is causally linked to many epithelial cancers, including breast cancer [2, 10, 11]. In *Drosophila* tumor models, EGF receptor (EGFR) overexpression drives hyperplastic growth, but the tissue does not normally progress to neoplasia [12]. When combined with additional genetic alterations, the hyperplastic imaginal disc tissues can undergo neoplastic transformation and metastasis [12–14]. Interestingly, specific genetic combinations produce tumors with different phenotypic characteristics, suggesting that these models may provide the means to explore specific cancer phenotypes.

A growing body of evidence has suggested an association between altered sugar metabolism and cancer risk [15–18]. In cancer cells, glucose metabolism shifts away from using pyruvate to feed oxidative phosphorylation toward use of lactate in aerobic glycolysis (the Warburg effect). The lactate dehydrogenase enzyme plays a key role in the shift to Warburg metabolism. Altered metabolism is thought to enhance the growth potential of cancer cells by diverting glucose to produce building blocks for increased biomass in the form of amino acids, at the expense of efficiency in ATP production via the tricarboxylic acid (TCA) cycle [19]. Depletion of lactate dehydrogenase (LDH) can reduce tumorigenesis in EGFR (Neu)-dependent breast cancer as well as c-Myc-mediated transformation [20, 21], indicating an important role for this metabolic shift. LDH was found to be upregulated in a *Drosophila* tumor model driven by overexpressing the activated vascular endothelial growth factor (VEGF) or platelet-derived growth factor (PDGF) receptor, Pvr [22], but its contribution to tumor formation was not assessed. In this report, we identify LDH as a cooperating factor that is both necessary and sufficient for EGFR-driven epithelial neoplasia *in vivo*. Genetic alterations that increase glucose flux, or a high-sugar diet, were sufficient to promote EGFR-driven neoplasia, and this depends on LDH. These findings provide evidence that Warburg effect metabolism may have a

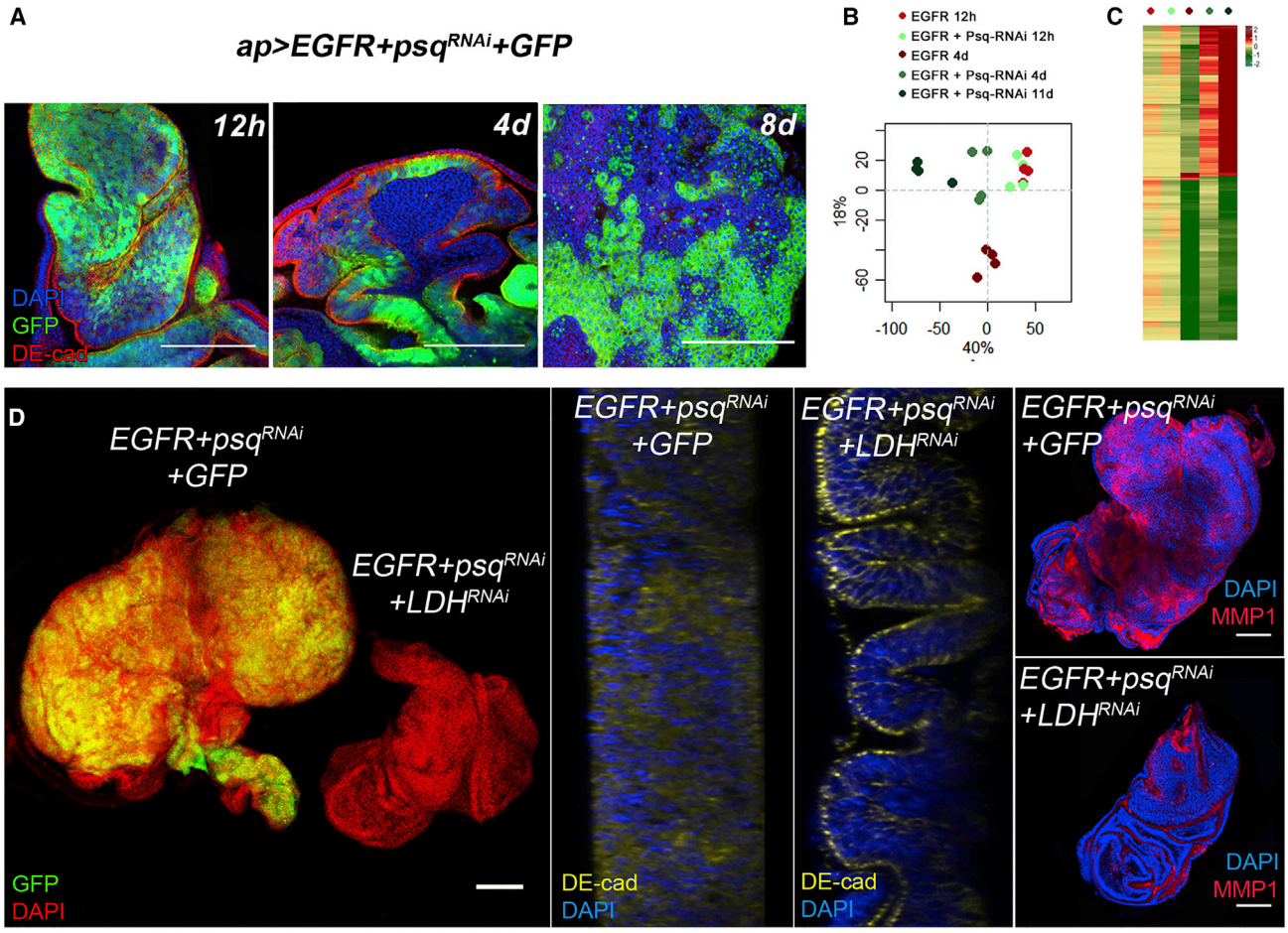

Figure 1. LDH Activity Required for EGFR-Induced Tumor Formation

(A) Confocal micrographs of wing imaginal discs expressing *UAS-EGFR+UAS-GFP* alone or together with *UAS-psq*^{RNAi} to deplete *psq*. Transgenes were activated using *apGal4* and *Gal80*^{ts} to control the timing of transgene expression, as described [13]. Discs were labeled with antibody to DE-cadherin (red) to label apical junctional complexes and DAPI (blue) to show the tissue. Samples were collected at 12 hr, 4 days, and 8 days after transgene induction for the *EGFR+psq*^{RNAi} genotype and at 12 hr and 4 days for *EGFR* alone. The scale bars represent 100 μm. See Figure S1A for quantification. See Figure S2 for relevant transcript expression data. See Table S1 for list of genes upregulated in neoplasia. See also Figure S3 for lactate measurement.

(B) Unsupervised principal-component analysis illustrating that replicate samples cluster together. PCA shows biological group separation according to time progression (1st component) and genetic background (2nd component; red versus green). The first two components account for 58% of variation in the data.

(C) Heatmap illustrating expression levels of the most important genes contributing to the 1st and 2nd PCA components. See Figure S2A for expression data on metabolic pathways.

(D) Imaginal discs expressing *UAS-EGFR+UAS-psq*^{RNAi} with *UAS-GFP* or *UAS-LDH*^{RNAi} under *apGal4* control to deplete LDH activity. Note the reduced size of the LDH depleted tissue. Middle panels show optical cross sections of discs labeled with anti-DE-cadherin. Right panels show other discs of the same genotypes labeled with antibody to MMP1 (red) and DAPI. The scale bars represent 100 μm.

See Figure S1B for quantification. Controls for RNAi are in Figure S2.

more fundamental role in driving neoplasia than previously appreciated.

RESULTS

In *Drosophila* imaginal discs, *EGFR* overexpression drives hyperplastic growth, but the tissue does not progress to neoplasia and metastasis. When combined with depletion of the chromatin regulator *pipsqueak* (*psq*), the hyperplastic imaginal disc tissue loses epithelial polarity, undergoes neoplastic transformation, and forms metastases [13]. To examine transcriptional changes during progression from hyperplasia to neoplasia, we examined a time course of progression after transgene induction in wing imaginal discs. At 4 days after transgene induction, both *EGFR* and *EGFR+psq*^{RNAi} genotypes produce hyperplastic tissue with overall normal epithelial organization, with normal apicobasal polarity (Figure 1A; quantification in Figure S1A). By 8 days, the *EGFR+psq*^{RNAi} discs have almost completely lost epithelial organization and continued to grow (Figures 1A and S1A), whereas those expressing *EGFR* alone have stopped growth and the larvae undergone pupariation.

RNA expression profiles were compared from imaginal discs expressing *EGFR* with or without the *psq*^{RNAi} transgene to deplete *psq*. Samples were collected in quadruplicate at 12 hr

and 4 days for the *EGFR*-expressing control hyperplastic tissue and at 12 hr, 4 days, and 11 days for the *EGFR+psq*^{RNAi} tumor samples (Figure 1A). The *EGFR* control and *EGFR+psq*^{RNAi} samples were very similar at the 12-hr time point (Figures 1B and 1C). The *EGFR+psq*^{RNAi} samples were different from the *EGFR* samples at 4 days and became more so by 11 days, with a set of transcripts showing progressive upregulation in the *EGFR+psq*^{RNAi} samples (Figures 1B and 1C). While this work was in progress, Wang et al. [22] reported that *Ecdysone-inducible gene L3* (*ImpL3*), which encodes *Drosophila* LDH, was upregulated along with other enzymes involved in glucose metabolism in a *Drosophila* tumor model driven by overexpressing the activated VEGF or PDGF receptor, *Pvr*. *LDH* was among the most upregulated genes in our 11-day *EGFR+psq*^{RNAi} tumor samples ($\log_2$ fold change 2.5; adjusted p value 0.001), along with several other genes involved in glucose and pyruvate metabolism (Figure S2A).

To test the contribution of *LDH* upregulation in the *EGFR+psq*^{RNAi} tumor model, we co-expressed an upstream activating sequence (UAS)-RNAi transgene to selectively deplete *LDH*. The ability of the RNAi transgene to offset upregulation of *LDH* transcript in the *EGFR+psq*^{RNAi} model was confirmed by qRT-PCR (Figure S2B). We also confirmed that depleting LDH alone had little or no effect on growth of normal tissue (Figure S1C). Depletion of *LDH* reduced tumor growth (Figures 1D and S1B) and restored normal epithelial organization in *EGFR+psq*^{RNAi} tumors, visualized by restored apical localization of the epithelial polarity marker DE-cadherin (Figure 1D). We confirmed that elevated *LDH* expression in these tumors correlated with an increase in lactate production and that depletion of *LDH* transcript offset this increase (Figure S3). Other transcripts tested had no effect on tumor formation in the *EGFR+psq*^{RNAi} model (Table S1).

Loss of epithelial organization and matrix metalloproteinase 1 (MMP1) expression are typically associated with transformation and invasiveness of human epithelial cancers and correlate with metastatic potential in imaginal disc tumor models [12, 23, 24]. We noted a strong reduction in the amount of MMP1 expression in the *LDH* depleted tissue, compared to the tissue expressing *EGFR+psq*^{RNAi} alone (Figure 1D). These findings suggest that *LDH* activity is required for the neoplastic transformation of the epithelial tissue in the *EGFR+psq*^{RNAi} model. It is noteworthy that depletion of *LDH* did not affect growth in another epithelial tumor model based on removing *scribble*, although *LDH* was upregulated in those tumors [25].

LDH Drives Neoplasia

A more detailed look at *LDH* transcript using qPCR showed a progressive increase in *LDH* levels in tissue expressing *EGFR+psq*^{RNAi}. At 4 days, when the tissue was hyperplastic in morphology, the difference was ~2-fold (Figure 2A). By 8 days, this increased >10-fold, as the tissue became neoplastic (Figure 2A). The finding that *LDH* expression was strongly upregulated during the transition from hyperplastic to neoplastic growth prompted us to ask whether *LDH* might be sufficient to push hyperplastic tissue into neoplasia. To address this, we used an EP line (a P element containing UAS sequences for Gal4 driven activation) inserted at the endogenous *ImpL3* gene to allow Gal4-dependent regulation of *LDH* (overexpression was confirmed by qPCR; Figure S2B). Although expression of *UAS-LDH* on its own caused a small reduction in average disc size (Figures 2B and S1D), co-expression of *LDH* with *EGFR* led to the formation of large tumors with elevated MMP1 expression compared to the *EGFR* control (Figures 2C, 2D, and S1E). The *EGFR+LDH* tumors also showed loss of epithelial polarity, visualized by loss of polarized DE-cadherin (Figure 2E). These tumors also showed disruption of the integrity of the basement membrane, visualized by loss of perlecan expression (Figure 2F). Interestingly, co-expression of *LDH* with the Hippo pathway transcriptional coactivator, *Yorkie*, or with an activated form of *Notch* also promoted tumor formation (Figure S1F). In each case, the underlying growth driver did not produce neoplasia on its own but can be pushed toward a more aggressive state by increased *LDH* activity.

Increased Glucose Intake Promotes Neoplasia

Glycolysis is considerably less efficient than oxidative phosphorylation in terms of ATP yield per molecule of glucose. To compensate for this, cancer cells increase glucose uptake by upregulating glucose transporters, including GLUT1 [26, 27]. In this context, it was interesting that *Glut1* transcript levels were lower in the neoplastic *EGFR+psq*^{RNAi} tumors compared to hyperplastic discs (Figure S2C). To test the effect of increased glucose flux, we expressed the *EGFR* transgene with and without a *UAS-Glut1* transgene. Increasing *Glut1* expression on its own had only a limited effect on disc size (Figure S1G), but when co-expressed with *EGFR*, *Glut1* produced massively overgrown imaginal discs (compare Figure 3A with 3C and 3E with 3F; measurements in Figure S1G). We observed the same effect by rearing the *EGFR*-expressing larvae on a high-sugar diet (compare Figure 3A with 3D and 3E with 3H and 3I; measurements in Figure S1H). Downregulation of *Glut1* might reflect a regulatory feedback mechanism designed to limit sugar uptake when the pyruvate shunt is active. This appears to protect against neoplasia. Indeed, further depletion of *Glut1* by RNAi treatment strongly reduced growth of the *EGFR+psq*^{RNAi} tumors (Figure S1I).

Co-expression of *UAS-Glut1* with *UAS-EGFR* led to loss of epithelial polarity, shown by delocalization of apical DE-cadherin (Figures 3E and 3F), but this was largely restored to normal by depleting *LDH* in this background (Figure 3G), and disc size was reduced toward normal (Figure S1G). Rearing larvae on a high-sugar diet was not in itself sufficient to compromise epithelial polarity, but when *EGFR*-expressing larvae were fed high sugar, polarity was lost (Figures 3H and 3I). Again, polarity was restored by *LDH* depletion in the high-sugar model (Figure 3J), and disc size was reduced (Figure S1G). In both cases, the effects of elevated sugar flux are mediated via *LDH* activity, suggesting a link to aerobic glycolysis. In a different *Drosophila* genetic model, a high-sugar diet increased the aggressiveness of tumors produced by expression of oncogenic *Ras* and activation of *Src* [28]. In this model, the transformed tissue responds to high sugar by promoting insulin sensitivity. The mechanism appears to be different from the *EGFR* model in which downregulation of *Glut1* appears to form part of a feedback mechanism to limit sugar flux via the pyruvate shunt.

Our findings provide evidence that elevated sugar flux can drive cells toward a neoplastic phenotype. We noted that animals with increased *LDH* activity, animals with increased *Glut1* expression, and those fed with increased dietary sugar

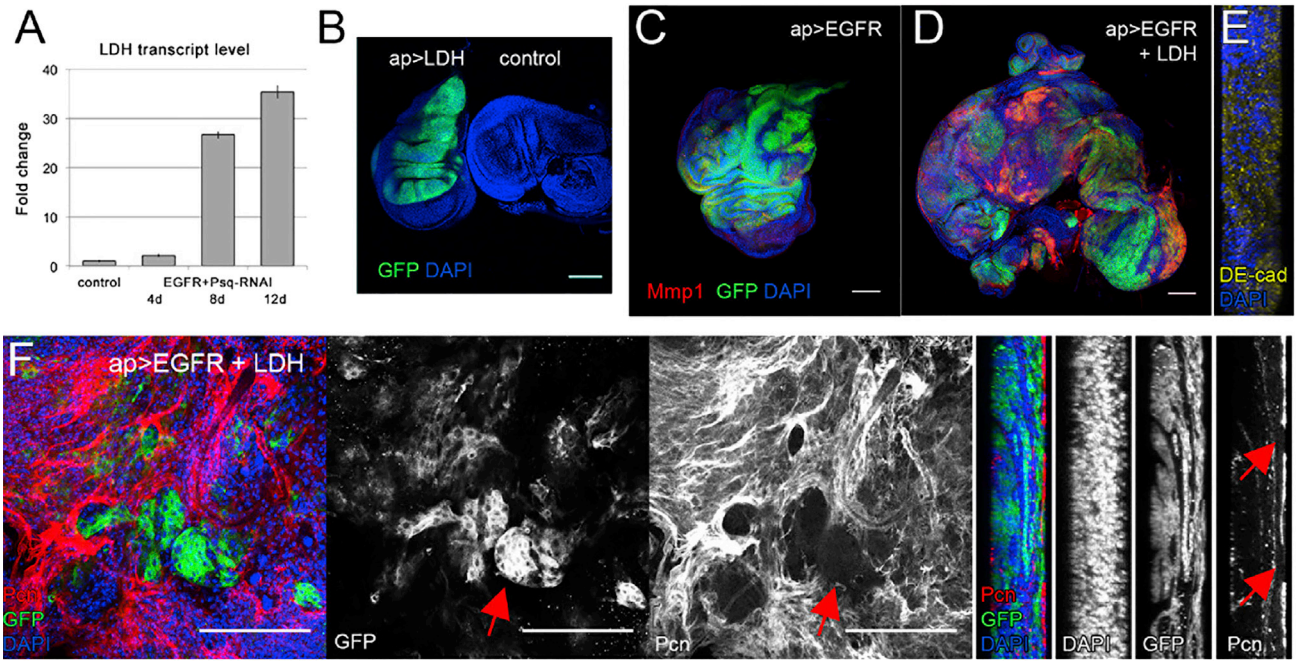

Figure 2. LDH Cooperates with EGFR to Drive Neoplastic Tumor Formation

(A) LDH mRNA measured by qPCR. *apGal4* was used to drive *UAS-EGFR* + *UAS-psq*^{RNAi} for 4, 8, and 12 days. Control is *apGal4* + *UAS-GFP* at 4 days. The data show mean ± SD from three technical replicates of a representative experiment. Comparable results were obtained in independent experiments. Data were normalized to α*Tub84B*.

(B) *apGal4*-driven expression of an EP-transgene insertion at the *Impl3* locus was used to direct LDH expression. LDH overexpression was verified by qPCR (see Figure S2B).

(C and D) Discs expressing *EGFR* alone (C) or with *LDH* (D) under *apGal4* control. Discs were labeled with antibody to MMP1 (red), DAPI, and GFP. See Figure S1D for size measurements.

(E and F) Discs expressing *EGFR*, *GFP*, and *LDH*.

(E) Optical cross section (XZ) labeled with antibody to DE-cadherin and DAPI.

(F) XY and XZ optical sections labeled with GFP, DAPI, and antibody to perlecan to label the basement membrane. Arrows indicate gaps where the basement membrane has broken down.

Scale bars represent 100μm.

contained small patches of GFP-expressing tissue in their body cavity, at some distance from the primary tumorous imaginal disc (boxed regions shown at higher magnification in Figures 3A–3D). In light of the loss of epithelial organization under these conditions, it is tempting to speculate that these may represent metastatic lesions originating from the primary tumor as a consequence of cellular transformation induced by high levels of aerobic glycolysis.

LDH Promotes a Transformed Phenotype in a Human Breast Cancer Model

A previous study reported that increased GLUT3 expression increased the transformed phenotype in a 3D breast cancer culture model [29]. We asked whether elevated LDH activity was sufficient to promote a transformed phenotype using a breast epithelial cell line derived from normal tissue. HTM3522 cells were transduced to express human LDHA or with a control vector and assayed in culture and in a 3D matrix. In 2D culture, cells overexpressing LDHA become spindle shaped and formed fewer coherent islets (Figure 4A). These shape changes are reminiscent of an epithelial-mesenchymal transition. Consistently, LDHA was among the RNAs reported to be upregulated in MCF10A breast cancer cells undergoing epithelial-mesenchymal transition (EMT) [30]. In 3D culture, cells treated with the control vector formed tight acinar spheres, with normal apico-basal polarity (apical inward, visualized by labeling with the Golgi marker GM130; Figures 4B and 4C). This polarized organization was lost in ~1/3 of the samples expressing LDHA (Figures 4B–4D). This difference was statistically significant ($p = 0.0158$; odds ratio 2.07 using Fisher's exact test).

Interestingly, increased glucose transporter levels have been reported to promote a transformed phenotype, reducing epithelial polarization in 3D cultures of breast cancer cells, and these phenotypes were suppressed by lowering glucose transporter levels [29]. Together with our findings, this study prompted us to ask whether increased sugar flux through the glycolytic pathway might be linked to poor clinical outcome in human cancers.

Synergy between LDHA and EGFR in Human Cancer

To examine links between LDH and EGFR in human cancers, we made use of publically available data from The Cancer Genome Atlas (TCGA). 20 cancer types had RNA sequencing data available for at least 100 patients and sufficient clinical follow-up to

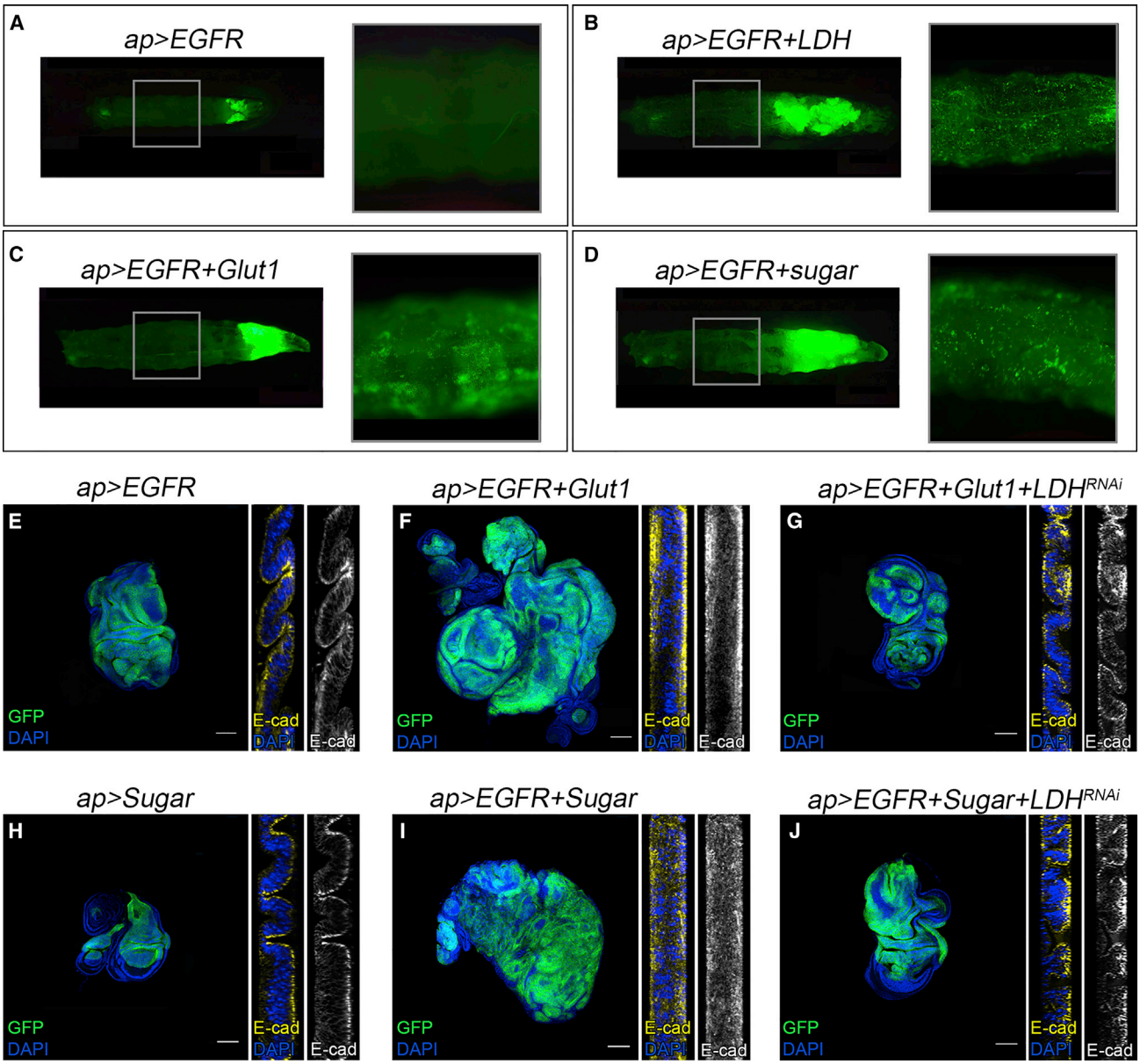

Figure 3. High Sugar Causes Neoplasia in EGFR-Expressing Discs

(A–D) Images of whole larvae expressing *UAS-EGFR* and *UAS-GFP* under *apGal4* control. Shown are Ap-Gal4+UAS-EGFR (A), Ap-Gal4+UAS-EGFR+UAS-LDH (B), Ap-Gal4+UAS-EGFR+UAS-Glut1 (C), and Ap-Gal4+UAS-EGFR (D) fed on high sugar diet.

(B–D) Co-expressing *EP-LDH* (B); co-expressing *UAS-Glut1* (C) fed on a high-sugar diet (D). The boxed area is shown magnified at right in each panel.

(E–G) Imaginal discs from larvae expressing *UAS-EGFR* and *UAS-GFP* under *apGal4* control. Shown are Ap-Gal4+UAS-EGFR (E), Ap-Gal4+UAS-EGFR+UAS-Glut1 (F), and Ap-Gal4+UAS-EGFR+UAS-Glut1+ UAS-LDH^{RNAi} (G).

(F) Co-expressing *UAS-Glut1*.

(G) Co-expressing *UAS-Glut1* and *UAS-LDH^{RNAi}*. See Figure S1G for size measurements.

(H and I) *apGal4* alone (H) or expressing *UAS-EGFR* (I) and fed on a high-sugar diet.

(J) *apGal4* + *UAS-EGFR* co-expressing *UAS-LDH^{RNAi}* and fed on a high-sugar diet. See Figure S1H for size measurements. See Figure S3 for Glut1 mRNA PCR. Scale bars represent 100μm.

reveal disease progression in at least 10% of patients. These cancers were selected for analysis (patient information is summarized in Table S2). Human LDH enzymes are encoded by 4 genes. The LDHA isoform favors conversion of pyruvate to lactate, whereas LDHB favors conversion of lactate to pyruvate. LDHA expression is elevated in many cancers due to hypoxia-induced upregulation, and LDHB is often downregulated [31]. We therefore determined the ratio of LDHA/LDHB expression for each cancer type and divided the patient populations into 3 equal-sized groups (low, middle, and high). Next, we estimated EGFR activity in these cancers using TCGA protein expression data for total EGFR plus the pY1068 and pY1173 tyrosine

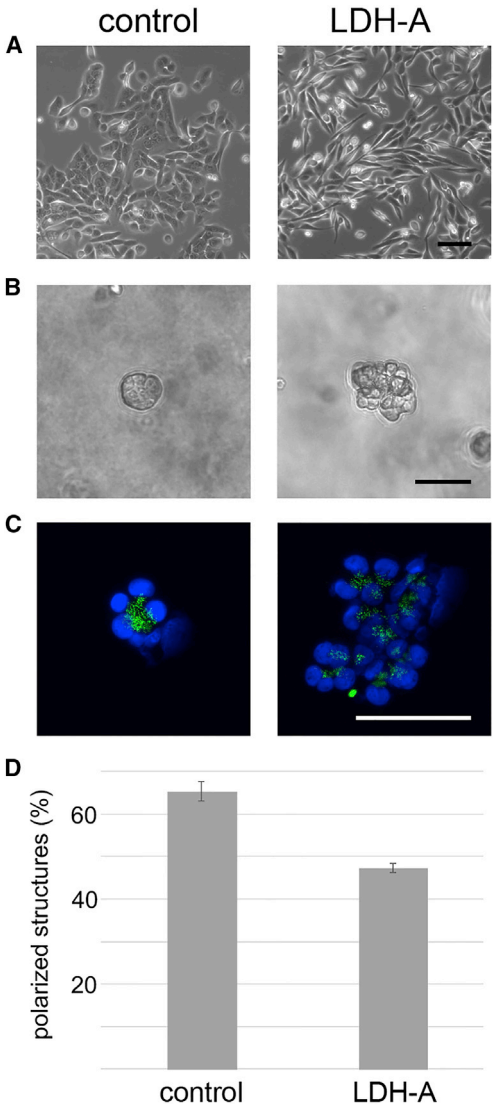

Figure 4. Elevated LDHA Compromises Polarity in Human Breast Epithelia

Cells were transduced to express LDHA or with a control vector. LDHA expression was verified by qPCR.

(A) Phase contrast imaging of monolayer cultures. The scale bar represents 100 μm.

(B) Phase contrast imaging 3D Matrigel cultures. The scale bar represents 50 μm.

(C) Immunostaining with the Golgi marker GM130 (green). Nuclei were labeled with DAPI (blue). The scale bar represents 50 μm.

(D) Graphs show the mean value of the percentage of apically polarized structures in three separate experiments ± SD.

phosphorylated forms of EGFR and divided the patients in groups based on EGFR level. Where patient numbers were insufficient for 3 groups, low versus high groups were used, as indicated in Table S2.

To test the hypothesis that there might be synergy between a shift toward high LDHA/B ratio and elevated EGFR activity, we performed a multivariate regression analysis and calculated the hazard ratio (HR) for synergistic effects progression. In the case of three cancer types (breast cancer [BRCA estrogen receptor (ER)/progesterone receptor (PR) negative], sarcoma [SARC], and lower grade glioma [LGG]; Figure 5A), there was a significant effect on progression-free survival, as indicated by the increased HR. For these three cancer types, we plotted an effect size for LDHA/B ratio, EGFR levels, and the combined effects separately (Figures 5B–5D). For all 3 cancer types, the patient subgroup with both high EGFR levels and high LDHA/B ratio showed an increased HR, and those with middle or low levels did not (Figures 5B–5D). For LGG, high EGFR and high LDHA/B ratio had no effect on their own. Interestingly, for sarcoma, the high EGFR group on its own showed a reduced hazard ratio but clearly synergized with high LDHA/B ratio to result in a worse outcome (Figure 5C). The breast cancer patients were placed into two groups due to the lower number of hormone-receptor-negative patients with clinical events. Notably, the high LDHA/B group on its own showed a reduced hazard ratio but clearly synergized with high EGFR to result in a worse outcome (Figure 5D). These findings provide evidence that patients with both higher LDHA activity and higher EGFR activity show earlier disease progression in breast cancer, sarcoma, and lower grade gliomas.

DISCUSSION

In this report, we identify the LDH enzyme as a critical factor driving the transition from benign hyperplastic growth to neoplasia and metastasis in an EGFR-dependent *Drosophila* epithelial tumor model. LDH upregulation was needed for EGFR-dependent neoplasia. Moreover, LDH overexpression was sufficient to drive neoplasia in combination with EGFR expression. Overexpression of LDHA in a human primary breast cancer cell model promoted a more transformed cellular phenotype. The possible significance of synergy between high LDH in a background of high EGFR activity in human cancer is supported by our analysis of TCGA datasets: we report evidence that patients with higher LDHA activity and higher EGFR activity show earlier disease progression in breast cancer, sarcoma, and lower grade gliomas. These effects were only seen when the two factors occurred together, suggesting synergy between EGFR activity and the metabolic shift toward aerobic glycolysis.

While this manuscript was in preparation, another study reported that increases in LDHA were able to promote EMT and invasiveness in renal clear cell carcinoma (ccRCC) and that blocking LDH activity could suppress these phenotypes as well as metastasis of ccRCC in xenografts [32]. Although we find no evidence for an effect of LDHA alone or of LDHA/EGFR synergy in the TCGA ccRCC data, these findings merit further attention.

The observations reported here provide evidence that increased sugar flux, whether dietary or due to increased absorption, can promote neoplastic transformation of *EGFR*-expressing epithelial tissue. The underlying metabolic changes appear to elicit these effects via the lactate shunt, because the effects of high sugar were abrogated by lowering the level of LDH expression in the tissue. A number of recent studies have begun to link elevated sugar flux to the metastatic phenotype [29, 32]. Together with our findings, these studies may provide

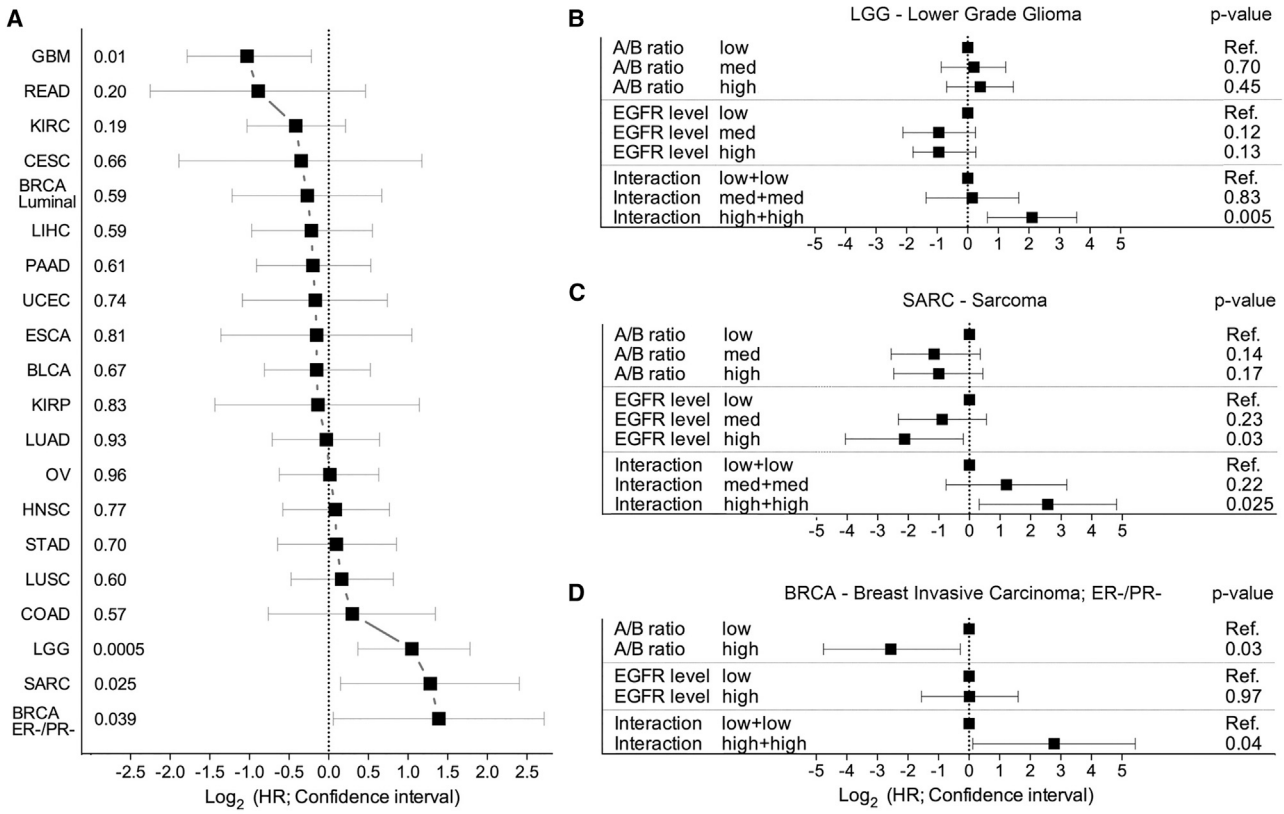

Figure 5. LDH Activity Synergizes with EGFR in Human Cancers

Forest plots representing multivariate Cox proportional hazard regression models, illustrating variable effect size on progression-free survival. Filled squares represent the hazard ratio (HR); lines represent the confidence interval.

(A) Forest plot showing HR for the synergy between increased LDHA/LDHB ratio and increased EGFR levels.

(B–D) Forest plots showing HR for increased LDHA/LDHB ratio and EGFR levels independently and when interacting. Shown are LGG (B), SARC (C), and BRCA (D).

Vertical line, reference line; x axis, $\log_2$ hazard ratio and confidence interval; y axis, abbreviation for TCGA cancer type. Data were adjusted for histopathological parameters as indicated in Table S2.

a molecular framework to better understand the links between diet, obesity, and cancer [16–18] and may help to select patient populations who might benefit from future therapeutic agents targeting lactate dehydrogenase activity.

STAR★METHODS

Detailed methods are provided in the online version of this paper and include the following:

- KEY RESOURCES TABLE
- CONTACT FOR REAGENT AND RESOURCE SHARING
- EXPERIMENTAL MODEL AND SUBJECT DETAILS
  - Drosophila melanogaster strains
  - Genotypes of experimental models
  - Controlled Overgrowth using Gal80^{ts}
  - Cell lines
- METHOD DETAILS
  - RNA extraction and microarrays
  - Microarray data analysis
  - Quantitative PCR
  - Immunostaining
  - LDHA expression, cell culture, viral transduction
  - 3D Epithelial polarization assay
  - Computational analysis of human tumor data
  - Lactate measurement
- QUANTIFICATION AND STATISTICAL ANALYSIS
  - Imaginal Disc Size Quantification
  - Hazard Ratio
- DATA AND SOFTWARE AVAILABILITY

SUPPLEMENTAL INFORMATION

Supplemental Information includes three figures and two tables and can be found with this article online at https://doi.org/10.1016/j.cub.2018.08.035.

ACKNOWLEDGMENTS

This work was funded by grants from the NovoNordisk Foundation (NNF12OC0000552) and the Neye Foundation to S.M.C. and by the Innovation Fund Denmark (0603-00320B) to J.G. F.C.P.F. was supported by a fellowship from the National Council of Scientific and Technological Development, Brazil (CNPq, 204675/2014-6).

AUTHOR CONTRIBUTIONS

T.E., R.V., F.C.P.F., B.I.A., and H.H. did the experiments. H.T.N. generated the viruses. D.A. performed the computational analysis. T.E., R.V., D.A., J.G., O.W.P., H.H., and S.M.C. analyzed the data. T.E., D.A., H.H., and S.M.C. wrote the manuscript. S.M.C. acquired funding.

DECLARATION OF INTERESTS

The authors declare no competing interests.

Received: November 20, 2017
Revised: May 21, 2018
Accepted: August 15, 2018
Published: October 4, 2018

REFERENCES

1. Stratton, M.R. (2011). Exploring the genomes of cancer cells: progress and promise. Science *331*, 1553–1558.
2. Kandoth, C., McLellan, M.D., Vandin, F., Ye, K., Niu, B., Lu, C., Xie, M., Zhang, Q., McMichael, J.F., Wyczalkowski, M.A., et al. (2013). Mutational landscape and significance across 12 major cancer types. Nature *502*, 333–339.
3. Navin, N.E. (2014). Cancer genomics: one cell at a time. Genome Biol. *15*, 452.
4. Tellez-Gabriel, M., Ory, B., Lamoureux, F., Heymann, M.F., and Heymann, D. (2016). Tumour Heterogeneity: The Key Advantages of Single-Cell Analysis. Int. J. Mol. Sci. *17*, E2142.
5. Brumby, A.M., and Richardson, H.E. (2003). scribble mutants cooperate with oncogenic Ras or Notch to cause neoplastic overgrowth in Drosophila. EMBO J. *22*, 5769–5779.
6. Pagliarini, R.A., and Xu, T. (2003). A genetic screen in Drosophila for metastatic behavior. Science *302*, 1227–1231.
7. Gonzalez, C. (2013). Drosophila melanogaster: a model and a tool to investigate malignancy and identify new therapeutics. Nat. Rev. Cancer *13*, 172–183.
8. Herranz, H., Eichenlaub, T., and Cohen, S.M. (2016). Cancer in Drosophila: Imaginal Discs as a Model for Epithelial Tumor Formation. Curr. Top. Dev. Biol. *116*, 181–199.
9. Copeland, N.G., and Jenkins, N.A. (2010). Harnessing transposons for cancer gene discovery. Nat. Rev. Cancer *10*, 696–706.
10. Paez, J.G., Jänne, P.A., Lee, J.C., Tracy, S., Greulich, H., Gabriel, S., Herman, P., Kaye, F.J., Lindeman, N., Boggon, T.J., et al. (2004). EGFR mutations in lung cancer: correlation with clinical response to gefitinib therapy. Science *304*, 1497–1500.
11. Sibilia, M., Kroismayr, R., Lichtenberger, B.M., Natarajan, A., Hecking, M., and Holcmann, M. (2007). The epidermal growth factor receptor: from development to tumorigenesis. Differentiation *75*, 770–787.
12. Herranz, H., Hong, X., Hung, N.T., Voorhoeve, P.M., and Cohen, S.M. (2012). Oncogenic cooperation between SOCS family proteins and EGFR identified using a Drosophila epithelial transformation model. Genes Dev. *26*, 1602–1611.
13. Herranz, H., Weng, R., and Cohen, S.M. (2014). Crosstalk between epithelial and mesenchymal tissues in tumorigenesis and imaginal disc development. Curr. Biol. *24*, 1476–1484.
14. Eichenlaub, T., Cohen, S.M., and Herranz, H. (2016). Cell Competition Drives the Formation of Metastatic Tumors in a Drosophila Model of Epithelial Tumor Formation. Curr. Biol. *26*, 419–427.
15. Cairns, R.A., Harris, I.S., and Mak, T.W. (2011). Regulation of cancer cell metabolism. Nat. Rev. Cancer *11*, 85–95.
16. Renehan, A.G., Zwahlen, M., and Egger, M. (2015). Adiposity and cancer risk: new mechanistic insights from epidemiology. Nat. Rev. Cancer *15*, 484–498.
17. Pavlova, N.N., and Thompson, C.B. (2016). The Emerging Hallmarks of Cancer Metabolism. Cell Metab. *23*, 27–47.
18. García-Jiménez, C., Gutiérrez-Salmerón, M., Chocarro-Calvo, A., García-Martinez, J.M., Castaño, A., and De la Vieja, A. (2016). From obesity to diabetes and cancer: epidemiological links and role of therapies. Br. J. Cancer *114*, 716–722.
19. Vander Heiden, M.G., Cantley, L.C., and Thompson, C.B. (2009). Understanding the Warburg effect: the metabolic requirements of cell proliferation. Science *324*, 1029–1033.
20. Fantin, V.R., St-Pierre, J., and Leder, P. (2006). Attenuation of LDH-A expression uncovers a link between glycolysis, mitochondrial physiology, and tumor maintenance. Cancer Cell *9*, 425–434.
21. Shim, H., Dolde, C., Lewis, B.C., Wu, C.S., Dang, G., Jungmann, R.A., Dalla-Favera, R., and Dang, C.V. (1997). c-Myc transactivation of LDH-A: implications for tumor metabolism and growth. Proc. Natl. Acad. Sci. USA *94*, 6658–6663.
22. Wang, C.W., Purkayastha, A., Jones, K.T., Thaker, S.K., and Banerjee, U. (2016). In vivo genetic dissection of tumor growth and the Warburg effect. eLife *5*, e18126.
23. Uhlirova, M., and Bohmann, D. (2006). JNK- and Fos-regulated Mmp1 expression cooperates with Ras to induce invasive tumors in Drosophila. EMBO J. *25*, 5294–5304.
24. Cordero, J.B., Macagno, J.P., Stefanatos, R.K., Strathdee, K.E., Cagan, R.L., and Vidal, M. (2010). Oncogenic Ras diverts a host TNF tumor suppressor activity into tumor promoter. Dev. Cell *18*, 999–1011.
25. Bunker, B.D., Nellimoottil, T.T., Boileau, R.M., Classen, A.K., and Bilder, D. (2015). The transcriptional response to tumorigenic polarity loss in Drosophila. eLife *4*, e03189.
26. Jones, R.G., and Thompson, C.B. (2009). Tumor suppressors and cell metabolism: a recipe for cancer growth. Genes Dev. *23*, 537–548.
27. DeBerardinis, R.J., Lum, J.J., Hatzivassiliou, G., and Thompson, C.B. (2008). The biology of cancer: metabolic reprogramming fuels cell growth and proliferation. Cell Metab. *7*, 11–20.
28. Hirabayashi, S., Baranski, T.J., and Cagan, R.L. (2013). Transformed Drosophila cells evade diet-mediated insulin resistance through wingless signaling. Cell *154*, 664–675.
29. Onodera, Y., Nam, J.M., and Bissell, M.J. (2014). Increased sugar uptake promotes oncogenesis via EPAC/RAP1 and O-GlcNAc pathways. J. Clin. Invest. *124*, 367–384.
30. Yang, L., Hou, Y., Yuan, J., Tang, S., Zhang, H., Zhu, Q., Du, Y.E., Zhou, M., Wen, S., Xu, L., et al. (2015). Twist promotes reprogramming of glucose metabolism in breast cancer cells through PI3K/AKT and p53 signaling pathways. Oncotarget *6*, 25755–25769.
31. Porporato, P.E., Dhup, S., Dadhich, R.K., Copetti, T., and Sonveaux, P. (2011). Anticancer targets in the glycolytic metabolism of tumors: a comprehensive review. Front. Pharmacol. *2*, 49.
32. Zhao, J., Huang, X., Xu, Z., Dai, J., He, H., Zhu, Y., and Wang, H. (2017). LDHA promotes tumor metastasis by facilitating epithelial-mesenchymal transition in renal cell carcinoma. Mol. Med. Rep. *16*, 8335–8344.
33. Friedrich, M.V., Schneider, M., Timpl, R., and Baumgartner, S. (2000). Perlecan domain V of Drosophila melanogaster. Sequence, recombinant analysis and tissue expression. Eur. J. Biochem. *267*, 3149–3159.
34. Briand, P., Petersen, O.W., and Van Deurs, B. (1987). A new diploid non-tumorigenic human breast epithelial cell line isolated and propagated in chemically defined medium. In Vitro Cell. Dev. Biol. *23*, 181–188.
35. Besson, M.T., Dupont, P., Fridell, Y.W., and Liévens, J.C. (2010). Increased energy metabolism rescues glia-induced pathology in a Drosophila model of Huntington's disease. Hum. Mol. Genet. *19*, 3372–3382.
36. Go, M.J., Eastman, D.S., and Artavanis-Tsakonas, S. (1998). Cell proliferation control by Notch signaling in Drosophila development. Development *125*, 2031–2040.
37. Gentleman, R.C., Carey, V.J., Bates, D.M., Bolstad, B., Dettling, M., Dudoit, S., Ellis, B., Gautier, L., Ge, Y., Gentry, J., et al. (2004).

Bioconductor: open software development for computational biology and bioinformatics. Genome Biol. *5*, R80.

38. Carvalho, B., Bengtsson, H., Speed, T.P., and Irizarry, R.A. (2007). Exploration, normalization, and genotype calls of high-density oligonucleotide SNP array data. Biostatistics *8*, 485–499.
39. Lê, S., Josse, J., and Husson, F. (2008). FactoMineR: an R package for multivariate analysis. J. Stat. Softw. *25*, 1–18.
40. Ritchie, M.E., Phipson, B., Wu, D., Hu, Y., Law, C.W., Shi, W., and Smyth, G.K. (2015). limma powers differential expression analyses for RNA-sequencing and microarray studies. Nucleic Acids Res. *43*, e47.
41. Colaprico, A., Silva, T.C., Olsen, C., Garofano, L., Cava, C., Garolini, D., Sabedot, T.S., Malta, T.M., Pagnotta, S.M., Castiglioni, I., et al. (2016). TCGAbiolinks: an R/Bioconductor package for integrative analysis of TCGA data. Nucleic Acids Res. *44*, e71.
42. Briand, P., Nielsen, K.V., Madsen, M.W., and Petersen, O.W. (1996). Trisomy 7p and malignant transformation of human breast epithelial cells following epidermal growth factor withdrawal. Cancer Res. *56*, 2039–2044.
43. Irizarry, R.A., Bolstad, B.M., Collin, F., Cope, L.M., Hobbs, B., and Speed, T.P. (2003). Summaries of Affymetrix GeneChip probe level data. Nucleic Acids Res. *31*, e15.
44. Irizarry, R.A., Hobbs, B., Collin, F., Beazer-Barclay, Y.D., Antonellis, K.J., Scherf, U., and Speed, T.P. (2003). Exploration, normalization, and summaries of high density oligonucleotide array probe level data. Biostatistics *4*, 249–264.
45. Brummelkamp, T.R., Bernards, R., and Agami, R. (2002). A system for stable expression of short interfering RNAs in mammalian cells. Science *296*, 550–553.
46. Jorgens, D.M., Inman, J.L., Wojcik, M., Robertson, C., Palsdottir, H., Tsai, W.T., Huang, H., Bruni-Cardoso, A., López, C.S., Bissell, M.J., et al. (2017). Deep nuclear invaginations are linked to cytoskeletal filaments - integrated bioimaging of epithelial cells in 3D culture. J. Cell Sci. *130*, 177–189.
47. Therneau, T.M., and Grambsch, P.M. (2000). Modeling Survival Data: Extending the Cox Model (New York: Springer).

STAR★METHODS

KEY RESOURCES TABLE

REAGENT or RESOURCE	SOURCE	IDENTIFIER
Antibodies		
rabbit anti-Perlecan	Stefan Baumgartner	[33]
mouse anti-MMP1	Developmental Studies Hybridoma Bank	Ab# 3A6B4, Ab# 5H7B11, Ab# 3B8D12
EGFR	Cell Signaling Technologies	Cat#2232
EGFR_pY1068	Cell Signaling Technologies	Cat#2234
EGFR_pY1173	Abcam	ab32578
Bacterial and Virus Strains		
LHDA and control viruses	This study	N/A
Chemicals, Peptides, and Recombinant Proteins		
Alexa Fluor 635 phalloidin	Life Technologies	Cat#A34054
Corning Matrigel Growth Factor Reduced (GFR) Basement Membrane Matrix, Phenol Red-free, *LDEV-free,	Corning	Cat#356231
Critical Commercial Assays		
SsoFast EvaGreen reagents	Bio Rad	Cat#1725200
SuperScript III First-Strand Synthesis System	Invitrogen	Cat#18080051
Agilent Seahorse XF96 Cell culture microplate	Seahorse Biosciences-Agilent Technologies	Cat# 101085-004
Deposited Data		
Microarray data	Gene Expression Omnibus database	GEO: GSE95613
Experimental Models: Cell Lines		
HTM3522 breast epithelial cells	Lab of OW Petersen	[34]
Phoenix-AMPHO	ATCC	ATCC CRL-3213
Experimental Models: Organisms/Strains		
ap-Gal4: y[1] w[*]; P{w[+mC] = CCAP-GAL4.P}16/CyO	Bloomington *Drosophila* Stock Center	BDSC: 25685; FlyBase: FBst0025685
UAS-EGFR: y[1] w[*]; P{w[+mc] = UAS-Egfr.B}32-26-1	Bloomington *Drosophila* Stock Center	BDSC: 5368; FlyBase: FBst0005368
UAS-Glut1	Marie-Thérèse Besson	[35]
UAS-yki: w[*]; P{y[+t7.7] w[+mC] = UAS-yki.V5.O}attP2	Bloomington *Drosophila* Stock Center	BDSC: 28819; FlyBase: FBst0028819
UAS-N_i	Provided by Marco Milan	[36]
UAS-mCD8-GFP: y[1] w[*]; P{w[+mC] = UAS-mCD8::GFP.L}LL5, P{UAS-mCD8::GFP.L}2	Bloomington *Drosophila* Stock Center	BDSC: 5137, FlyBase: FBst0005137
UAS-LDH^{RNAi}: y[1] v[1]; P{y[+t7.7] v[+t1.8] = TRiP.HMS00039}attP2	Bloomington *Drosophila* Stock Center	BDSC: 33640, FlyBase: FBst0033640
EP-LDH: y[1] w[67c23]; P{w[+mC] y[+mDint2] = EPgy2}EY07426	Bloomington *Drosophila* Stock Center	BDSC: 16829, FlyBase: FBst0016829
UAS-psq^{RNAi}	Vienna *Drosophila* RNAi Center	KK: 106404, FlyBase: FBgn0004399
Oligonucleotides		
αTub84B forward: TGGGCCCGTCTGGACCACAA	This paper	N/A
αTub84B reverse: TCGCCGTCACCGGAGTCCAT	This paper	N/A
LDH forward: GCTGGTAGAGTACAGTCCCG	This paper	N/A
LDH reverse: GGACGAGTCCAAGTTGGTG	This paper	N/A
Glut1 forward: ACCGATTGGCTAACTGCATC	This paper	N/A
Glut1 reverse: CAGACAGGTGGAGGCTGAC	This paper	N/A
Software and Algorithms		
Bioconductor (release 3.6. with default options)	[37]	http://www.bioconductor.org/
R (release 3.4.3)	N/A	https://www.r-project.org

(*Continued on next page*)

Continued

REAGENT or RESOURCE	SOURCE	IDENTIFIER
oligo package (1.42.0, with default options)	[38]	http://www.bioconductor.org/packages/release/bioc/html/oligo.html
FactorMineR (1.40)	[39]	http://factominer.free.fr
Limma 3.34.9	[40]	https://bioconductor.org/packages/release/bioc/html/limma.html
TCGAbiolinks (2.8.3)	[41]	https://bioconductor.org/packages/release/bioc/html/TCGAbiolinks.html
R package "Survival" (2.42-6)	N/A	https://cran.r-project.org/web/packages/survival/index.html

CONTACT FOR REAGENT AND RESOURCE SHARING

Further information and requests for resources and reagents should be directed to and will be fulfilled by the Lead Contact, Stephen M. Cohen (scohen@sund.ku.dk).

EXPERIMENTAL MODEL AND SUBJECT DETAILS

Drosophila melanogaster strains

ap-Gal4, *UAS-EGFR*, *UAS-Glut1*, *UAS-yki*, *UAS-N$_i$*, *UAS-DC8-GFP*, *UAS-LDH^{RNAi}* and *EP-LDH* were obtained from the Bloomington *Drosophila* Stock Center. The Vienna *Drosophila* RNAi Center provided *UAS-psq^{RNAi}* (no. 106404). *UAS-Glut1* was from Marie-Thérèse Besson [35]. *UAS-N$_i$* was from Marco Milan [36]. Flies were raised on medium containing agar (8 g/l), Brewer's yeast (23.6 g/l), dextrose (50.8 g/l) and corn meal (58 g/l). For the high sugar diet, 75 g of sucrose/l were added to the basic recipe. Flies were raised at 25°C in plastic vials on a 12h/12h light dark cycle, in a controlled humidity environment, except for those used in temperature controlled Gal4 experiments as specified below. Tumors samples were collected from mature third instar larvae. The sex of the larvae was not determined. The Health/immune status cannot be determined for individual larvae. Larvae were not subjected to previous procedures. Larvae were drug and test naive.

Genotypes of experimental models

Figure 1

(A) *ap-Gal4, UAS-psq^{RNAi}/UAS-CD8-GFP; UAS-EGFR, tub-Gal80ts/+*

(B) EGFR corresponds to *ap-Gal4, UAS-CD8-GFP/+; UAS-EGFR, tub-Gal80ts/+*; and EGFR + Psq-RNAi corresponds to *ap-Gal4, UAS-psq^{RNAi}/UAS-CD8-GFP; UAS-EGFR, tub-Gal80ts/+*

(D) EGFR + psq^{RNAi} + GFP corresponds to *ap-Gal4, UAS-psq^{RNAi}/UAS-CD8-GFP; UAS-EGFR, tub-Gal80ts/+*; and EGFR + psq^{RNAi} + LDH^{RNAi} corresponds to *ap-Gal4, UAS-psq^{RNAi}/+; UAS-EGFR, tub-Gal80ts/UAS-LDH^{RNAi}*

Figure 2

(A) Control corresponds to *ap-Gal4, UAS-CD8-GFP/+*; tub-Gal80ts/+; EGFR + psq^{RNAi} corresponds to *ap-Gal4, UAS-psq^{RNAi}/UAS-CD8-GFP; UAS-EGFR, tub-Gal80ts/+*

(B) ap > LDH corresponds to *ap-Gal4, UAS-CD8-GFP; tub-Gal80ts/EP-LDH;* control corresponds to *yw.*

(C) *ap-Gal4, UAS-CD8-GFP/+; UAS-EGFR, tub-Gal80ts/+*

(D-F) *ap-Gal4, UAS-CD8-GFP/+; UAS-EGFR, tub-Gal80ts/EP-LDH*

Figure 3

(A, D, E, I) *ap-Gal4, UAS-CD8-GFP/+; UAS-EGFR, tub-Gal80ts/+*

(B) *ap-Gal4, UAS-CD8-GFP/+; UAS-EGFR, tub-Gal80ts/EP-LDH*

(C, F) *ap-Gal4, UAS-CD8-GFP/UAS-Glut1; UAS-EGFR, tub-Gal80ts/+*

(G) *ap-Gal4, UAS-CD8-GFP/UAS-Glut1; UAS-EGFR, tub-Gal80ts/UAS-LDH^{RNAi}*

(H) *ap-Gal4, UAS-CD8-GFP/+; tub-Gal80ts/+*

(J) *ap-Gal4, UAS-CD8-GFP/+; UAS-EGFR, tub-Gal80ts/UAS-LDH^{RNAi}*

Figure S1

(A) Control corresponds to *ap-Gal4, UAS-CD8-GFP/+*; tub-Gal80ts/+; EGFR corresponds to *ap-Gal4, UAS-CD8-GFP/+*; UAS-EGFR, tub-Gal80ts/+; and EGFR + Psq^{RNAi} corresponds to *ap-Gal4, UAS-psq^{RNAi}/UAS-CD8-GFP; UAS-EGFR, tub-Gal80ts/+*

(B) EGFR + Psq^{RNAi} corresponds to *ap-Gal4, UAS-psq^{RNAi}/UAS-CD8-GFP; UAS-EGFR, tub-Gal80ts/+*; EGFR + psq^{RNAi} + LDH^{RNAi} corresponds to *ap-Gal4, UAS-psq^{RNAi}/UAS-CD8-GFP; UAS-EGFR, tub-Gal80ts/UAS-LDH^{RNAi}*

(C) Control corresponds to *ap-Gal4, UAS-CD8-GFP/+; tub-Gal80ts/+*; LDH^{RNAi} corresponds to *ap-Gal4, UAS-CD8-GFP/+; tub-Gal80ts/UAS-LDH^{RNAi}*

(D) Control corresponds to *ap-Gal4, UAS-CD8-GFP/+; tub-Gal80ts/+*; EP-LDH corresponds to *ap-Gal4, UAS-CD8-GFP/+; tub-Gal80ts/EP-LDH*

(E) Control corresponds to *ap-Gal4, UAS-CD8-GFP/+; tub-Gal80ts/+*; EGFR corresponds to *ap-Gal4, UAS-CD8-GFP/+; UAS-EGFR, tub-Gal80ts/+*; EGFR + LDH corresponds to *ap-Gal4, UAS-CD8-GFP/+; UAS-EGFR, tub-Gal80ts/EP-LDH*

(F) Control corresponds to *ap-Gal4, UAS-CD8-GFP/+; tub-Gal80ts/+*; Yki corresponds to *ap-Gal4, UAS-CD8-GFP/+; UAS-Yki, tub-Gal80ts/+*; Yki + LDH corresponds to *ap-Gal4, UAS-CD8-GFP/+; UAS-Yki, tub-Gal80ts/EP-LDH*; Ni corresponds to *ap-Gal4, UAS-CD8-GFP/+; UAS-Ni, tub-Gal80ts/+*; Ni + LDH corresponds to *ap-Gal4, UAS-CD8-GFP/+; UAS-Ni, tub-Gal80ts/EP-LDH*

(G) Control corresponds to *ap-Gal4, UAS-CD8-GFP/+; tub-Gal80ts/+*; EGFR corresponds to *ap-Gal4, UAS-CD8-GFP/+; UAS-EGFR, tub-Gal80ts/+*; EGFR + Glut1 corresponds to *ap-Gal4, UAS-CD8-GFP/UAS-Glut1; UAS-EGFR, tub-Gal80ts/+*; EGFR + Glut1 + LDH^{RNAi} corresponds to *ap-Gal4, UAS-CD8-GFP/UAS-Glut1; UAS-EGFR, tub-Gal80ts/UAS-LDH^{RNAi}*; and Glut 1 corresponds to *ap-Gal4, UAS-CD8-GFP/UAS-Glut1; tub-Gal80ts/+*

(H) Control and control + sugar correspond to *ap-Gal4, UAS-CD8-GFP/+; tub-Gal80ts/+*; EGFR and EGFR + sugar correspond to *ap-Gal4, UAS-CD8-GFP/+; UAS-EGFR, tub-Gal80ts/+*; and EGFR + sugar + LDH^{RNAi} correspond to *ap-Gal4, UAS-CD8-GFP/+; UAS-EGFR, tub-Gal80ts/LDH^{RNAi}*

(I) EGFR + Psq^{RNAi} + GFP corresponds to *ap-Gal4, UAS-psq^{RNAi}/UAS-CD8-GFP; UAS-EGFR, tub-Gal80ts/+*; and EGFR + Psq^{RNAi} + Glut1^{RNAi} corresponds to *ap-Gal4, UAS-psq^{RNAi}/UAS-Glut1^{RNAi}; UAS-EGFR, tub-Gal80ts/+*

Figure S2

(A) E corresponds to *ap-Gal4, UAS-CD8-GFP/+; UAS-EGFR, tub-Gal80ts/+*; and EP corresponds to *ap-Gal4, UAS-psq^{RNAi}/UAS-CD8-GFP; UAS-EGFR, tub-Gal80ts/+*

(B) LacZ corresponds to *ap-Gal4, UAS-CD8-GFP/+; tub-Gal80ts/UAS-lacZ*; EGFR + Psqi + GFP corresponds to *ap-Gal4, UAS-psq^{RNAi}/UAS-CD8-GFP; UAS-EGFR, tub-Gal80ts/+*; EGFR + Psqi + LDHi corresponds to *ap-Gal4, UAS-psq^{RNAi}/UAS-LDH^{RNAi}; UAS-EGFR, tub-Gal80ts/+*; RFP corresponds to *ap-Gal4, UAS-CD8-GFP/+; tub-Gal80ts/UAS-RFP*; EP-LDH corresponds to *ap-Gal4, UAS-CD8-GFP/+; tub-Gal80ts/EP-LDH*; EP-LDH + LDHi corresponds to *ap-Gal4, UAS-CD8-GFP/UAS-LDH^{RNAi}; tub-Gal80ts/EP-LDH*; EGFR corresponds to *ap-Gal4, UAS-CD8-GFP/+; UAS-EGFR, tub-Gal80ts/+*; EGFR + Psq-RNAi corresponds to *ap-Gal4, UAS-psq^{RNAi}/UAS-CD8-GFP; UAS-EGFR, tub-Gal80ts/+;* and control corresponds to *ap-Gal4, UAS-CD8-GFP/+; tub-Gal80ts/+*

Figure S3

EGFR corresponds to *ap-Gal4, UAS-CD8-GFP/+; UAS-EGFR, tub-Gal80ts/+*; and EGFR + Psq^{RNAi} hyperplastic and EGFR + Psq^{RNAi} neoplastic corresponds to *ap-Gal4, UAS-psq^{RNAi}/UAS-CD8-GFP; UAS-EGFR, tub-Gal80ts/+;* and EGFR + psq^{RNAi} + LDH^{RNAi} *ap-Gal4, UAS-psq^{RNAi}/UAS-LDH^{RNAi}; UAS-EGFR, tub-Gal80ts/+;*

Controlled Overgrowth using Gal80^{ts}

The Gal4/Gal80 system was used to allow conditional transgene activation in order to bypass early lethality due to expression of *EGFR+psq^{RNAi}*. Embryos were collected for 24h (for microarray experiments) or 48h (for immunostaining) at 18°C and were allowed to develop at 18°C to maintain *Gal80*-dependent repression of *Gal4* until the larvae reached early third instar (5 days for immunostaining or 7 days for microarray experiments). Larvae were then transferred to 29°C to induce *Gal4* and raised for the indicated times. Larval gender was not considered.

Cell lines

HTM3522 breast epithelial cells (female) were cultured in H14 medium consisting of DMEM:F12 with 2 mM glutamine containing 250ng/mL insulin, 10ng/mL EGF, 10μg/mL transferrin, 2.6ng/mL sodium selenite, 10^{-10} M estradiol, $1.4x10^{6}$ M hydrocortisone and 5μg/mL prolactin as described [42].

Phoenix-Ampho cells were purchased from American Type Culture Collection. These were not further authenticated.

METHOD DETAILS

RNA extraction and microarrays

Approximately 20 pairs of wing discs were dissected and processed for total RNA extraction using Trizol (Life Technologies). RNA was prepared from dissected imaginal discs from four replicates of each of the five conditions: *EGFR* and *EGFR+psq^{RNAi}* at 12 hr; *EGFR* and *EGFR+psq^{RNAi}* samples at day 4, and from *EGFR+psq^{RNAi}* at day 11 of tumor growth. Expression profiling was performed with Genechip *Drosophila* Genome 1.0 Arrays (Affymetrix) by the Genomics Core Facility at European Molecular Biology Laboratory (Heidelberg, Germany). Samples were blinded to the Genomics Core Facility for profiling.

Microarray data analysis

Microarray data analysis was performed using R(3.4.3)/Bioconductor [37]. Robust Multi-array Average (RMA) algorithm [43, 44] was used to normalize variation between arrays and within probe sets and to improve data distribution by log2 transformation of intensity values as implemented in *oligo* (1.42.0) package in Bioconductor R (http://www.bioconductor.org/packages/release/bioc/html/oligo.html [38],). For downstream analysis control, background and spike-in probes were removed. As well as genes whose expression was below background detection threshold in at least 4 samples. Threshold was defined as 80% of anti-genomic (background

hybridization) probe intensity's. This is important since expression estimate may not be a reliable for these genes. To ask if the gene expression data separated samples according to biological groups, principal component analysis (PCA) was applied to scaled $\log_2$ data. We used the "FactoMineR" (1.40) package with default options [[39]]. Genes that exhibited variation in expression levels between time points or genetic groups were selected for PCA analysis (based on linear model fit; adj.p.val < 0.05)(Limma; 3.34.9 [40]). This removes non-informative signals. Genes that contributed to first (time) and second (groups) component (> 0.025) were selected and their expression levels were visualized as a heatmap. Data was scaled and centered relative to control samples. Genes differentially expressed in 4d versus 11d *EGFR+psq* ^{RNAi} tumors were identified using "Limma" package with default settings. A gene was considered differentially expressed when the Bonferroni corrected P value was < 0.05 and the $\log_2$ fold change > 1.5.

Metabolic pathway status was assessed by examining gene signatures associated with KEGG maps; Glycolysis/Gluconeogenesis (above phosphoenolpyruvate); TCA cycle; Fructose and mannose metabolism; Oxidative phosphorylation (first 4 complexes); Pyruvate metabolism; Fatty acid biosynthesis; Fatty acid degradation. Normalized gene expression data was scaled and centered relative to control samples.

Quantitative PCR

20 wing imaginal discs from 3rd instar larvae were dissected in ice-cold PBS and were incubated in 1000 μl TRIzol (Invitrogen) for 5 min at room temperature. After the addition of 200 μl Chloroform, samples were vortexed vigorously for at least 15 s and incubated at room temperature for 3 min. The sample was centrifuged at 12000 g for 15 minutes at 4°C. Following centrifugation, the mixture separated into lower red, the phenol-chloroform phase, an interphase, and a colorless upper aqueous phase. RNA remains exclusively in the aqueous phase. The upper aqueous phase (~350 μl) was carefully transferred into fresh tube without disturbing the interphase. The RNA was precipitated from the aqueous phase by mixing it with 500 μl isopropyl alcohol. After 10 min incubation at room temperature, the sample was centrifuged at 12000 g for 10 min at 4°C. The RNA precipitate, often invisible before centrifugation, forms a gel-like pellet on the bottom of the tube. The pellet is washed with 1ml 75% ethanol. After centrifugation (7500 g, 5 min, 4°C), supernatant is removed completely and the pellet is air-dried for 5-10 min. RNA is resuspended in 30 μl sterile water. Up to 3 μg total RNA was treated with RQ1 DNase I (Promega) and reverse-transcribed using the SuperScript® III Reverse Transcriptase Kit and oligo(dT) Primer. For RNA denaturation, 1 μl of the primers, 1 μl 10mM dNTPs and the DNase-treated RNA were first incubated in a reaction volume of 13 μl for 5 min at 65°C and cooled down on ice. Next, 4 μl 5x First-Strand Buffer, 1 μl 0.1 M DTT, 1 μl of RNaseOUT RNase Inhibitor and 1 μl Superscript III RT (200 units/μl) were added. The reaction mix was incubated at 50°C for 60 min and inactivated at 70°C for 10 min. Real-time quantification was performed using SsoFastTM EvaGreen reagents (Bio-Rad) on QuantStudio 6 Flex Real-Time PCR System (Applied Biosystem). Primer Sequences:

αTub84B forward: TGGGCCCGTCTGGACCACAA
αTub84B reverse: TCGCCGTCACCGGAGTCCAT
LDH forward: GCTGGTAGAGTACAGTCCCG
LDH reverse: GGACGAGTCCAAGTTGGTG
Glut1 forward: ACCGATTGGCTAACTGCATC
Glut1 reverse: CAGACAGGTGGAGGCTGAC

Samples were not blinded. No data were excluded.

Immunostaining

Primary antibodies: rabbit anti-Perlecan (provided by Stefan Baumgartner [33]); anti-DE-Cadherin, and mouse anti-MMP1 (3A6B4/5H7B11/3B8D12 antibodies were mixed in equal amounts) were from Developmental Studies Hybridoma Bank. Alexa Fluor 635 phalloidin was used to label F-actin (Life Technologies). Third-instar larvae were dissected in PBS and fixed in 4% formaldehyde/PBS for 20' RT then washed three times for 10' in 0.1%Triton/PBS (PBT) and blocked for 30' in 3% BSA in PBT, 5mM NaCl (BBT). Samples were incubated at 4°C overnight with primary antibody diluted in BBT, washed three times for 15' in BBT, and incubated with fluorescent secondary antibody and DAPI for 1h RT. After four 15' washes with PBT, discs were mounted in 90% glycerol and PBS containing 0.05% N-Propyl Gallate. Samples were not randomized or blinded. Key experiments were repeated several times by 2 investigators with independent crosses over a period of years with consistent results. Samples were not blinded. For quantification, at least 10 larvae were dissected and analyzed as described below.

LDHA expression, cell culture, viral transduction

The LDHA-expressing construct was cloned by PCR using cDNA from HMT3522 cells into the pBabe (puro) expression vector with the primers ATGCAGATCTAATATGGCAACTCTAAAGGATC and GCGAGTCGACTTAAAATTGCAGCTCCTTTTGG. The plasmid was sequenced to verify the ORF (NM_005566). Phoenix-Ampho cells were cultured in DMEM media. Amphotropic retroviruses were made as described previously [45]. Viral particles-containing supernatant from transfected Phoenix-Ampho cells was harvested at 36–48 hr. HMT3522 cells were plated in H14 media 24 hours before being infected with viruses expressing LDHA or control empty vector overnight in the presence of 8 μg/ml polybrene. Puromycin (1μg/ml) selection was started at 36 hours and stable cells were obtained after 3 days.

3D Epithelial polarization assay

In monolayer culture, the HTM3522 breast epithelial cells were propagated on collagen coated culture vessels (Purecol; Advanced BioMatrix, San Diego, CA). Transductions were performed at passage 38. HMT3522-LDHA+ and HMT3522-EV were trypsinized to single cells from monolayer cultures and $1x10^5$ cells were embedded in 300μL Matrigel (BD Biosciences) in 24 well dishes in triplicate. From day 7 EGF was omitted from the H14 culture medium [46]. At day 12 the 3D gels were briefly dehydrated and snap frozen in −80° hexane. 10μm sections were cut on a cryostat with an interval of ≥ 30μm and fixed in 3.5% formalin, methanol/acetone 1:1 and 0.1% Triton X-100 for 5 min followed by staining with an antibody to the Golgi marker GM130 (clone 35/GM130, diluted 1:50/1:15, BD Biosciences) and visualized utilizing the Ultravision ONE Detection System (Thermo Fisher) for quantification, or by immunofluorescence with Alexa Flour 488 goat anti-mouse secondary antibodies (Invitrogen). The fraction of polarized structures was determined by evaluating structures consisting of > 4 cells in sections and scoring for the orientation of the GM130 staining as toward the lumen (polarized) or scattered (non-polarized). One hundred structures were examined for each gel. Samples were not blinded. No data were excluded.

Computational analysis of human tumor data

RNA sequencing data and clinical information were downloaded from The Cancer Genome Atlas (TCGA) Genomic Data Commons Data Portal (Data Release version 8.0) (https://gdc-portal.nci.nih.gov/), using the R package ''TCGAbiolinks'' [41]. Upper quartile normalized fragments per Kb of transcript per million mapped reads data was used for the analyses. Cancer types were selected by (1) RNA sequencing data available for at least 100 patients and (2) with sufficient follow-up to identify a clinical progression event in at least 10% of patients. 20 cancer types met these criteria and Progression free survival was calculated using data downloaded on 17.08.2017 (Table S2). Next, reverse phase protein array data were downloaded from http://tcpaportal.org/tcpa/ on 12.10.2017. Scaled level 4 relative protein levels of EGFR (Cell Signaling Technologies; 2232), EGFR_pY1068 (CST; 2234), EGFR_pY1173 (Abcam; ab32578) were summed to calculate an overall EGFR score. Acute Myeloid Leukemia did not have EGFR protein data, and was excluded from the analysis. To monitor the shift to LDHA activity we calculated the LDHA/LDHB expression ratio. For regression analysis patients were divided into equally sized groups (low, middle, high) based on overall EGFR score and on LDHA/LDHB ratio (Table S2; Figure S4). Multivariate regression analysis with interaction term was used to examine the relationship between progression free survival, overall EGFR levels and the shift toward LDHA metabolism [47]. The R package ''Survival'' was used to calculate Hazard Ratio and associated p value (https://cran.r-project.org/web/packages/survival/index.html).

Lactate measurement

ECAR was monitored using real-time assessment with the Seahorse XF^e96 Extracellular Flux Analyzer (Seahorse Biosciences-Agilent Technologies, USA) as a measure of lactic acid release to the extracellular medium. wing discs of the indicated genotypes were dissected in unbuffered DMEM (Sigma S5030) supplemented with 12 mM glutamine (pH 7.4) and placed in a Seahorse 96-well microplate (3 discs per well from control, *EGFR*, $EGFR{+}psq^{RNAi}{+}LDH^{RNAi}$ larvae, or 2 discs per well from $EGFR{+}psq^{RNAi}$). Experiments were also conducted in Schneider's Insect Medium (Sigma S9895) with similar results. Immediately after dissection, the plate was centrifuged at 300xg for 3-5 min to pull-down the disks to the bottom of the wells, and the analysis was performed. Each measurement cycle consisted of 1-min mix and 3-min measurement of the extracellular proton content. The analysis of lactate production and release was initiated by three baseline ECAR measurement cycles. These were followed by the sequential injection of 10 mM glucose to provide a substrate for cellular pyruvate production and subsequent lactate synthesis via LDH. Three ECAR measurement cycles were taken in between each injection and five final measurement cycles after the injection of 100 mM 2-Deoxyglucose to halt glycolytic function and ensure that responses in ECAR are due to lactate release and exclude non-glycolytic extracellular acidification. The pH of the reagents used during the test was adjusted to 7.4. The ECAR and OCR were recorded and calculated by the Seahorse XF^e96 software, Wave. To normalize the data, the protein content for each well was measured using the Pierce BCA assay with BSA as standard. Samples were blinded to the Seahorse system operator.

QUANTIFICATION AND STATISTICAL ANALYSIS

Imaginal Disc Size Quantification

Images were taken using a Leica SP8 confocal microscope and analyzed using Fiji software and Adobe Photoshop. Images of whole larvae were taken with a Leica M165 FC stereomicroscope equipped with GFP fluorescence optics. Images were processed with ImageJ and Adobe Photoshop CC. The orientation and/or position of the wing discs were adjusted for consistent orientation in the figures. No relevant information was affected. The original images are available on request. Wing imaginal discs of third instar larvae were dissected and stained with DAPI. Whole wing disc area was determined with ImageJ, by setting the threshold to include the whole DAPI-positive area with the option ''Threshold.'' The size of at least 10 discs per genotype was measured and statistical significance was determined by using the Mann–Whitney U test with Bonferroni adjustment for multiple comparisons using Graph Pad Prism. Data are in Figures S1 and S2. Many additional samples were visually examined, but not measured.

Hazard Ratio

The R package ''Survival'' was used to calculate Hazard Ratio and associated p value (https://cran.r-project.org/web/packages/survival/index.html). All covariates were tested and satisfied the proportional hazard assumption. To estimate most accurate effect

size all groups were treated as ordered factors and adjusted for classical histopathology parameters as indicated in Table S2. Patients with complete information on time to an event, status, histopathology parameters used for adjustment, LDHA/LDHB expression levels and EGFR protein levels were included in the regression analysis. A linear Cox proportion hazard regression model with ''contr. poly'' contrast was used to calculate interaction hazard ratio and p value. Contrast was set to ''contr.treatment'' in order to visualize the effect size for increase in overall EGFR level and increase in LDHA shift separately and for their interaction. Statistical analyses were performed using R Software and results were visualized as forest plots using GraphPad Prism.

DATA AND SOFTWARE AVAILABILITY

The accession number for the microarray data reported in this paper is GEO: GSE95613.